Asymmetric Distribution of Lunar Impact Basins Caused by Variations in Target Properties

Katarina Miljković,[1]* Mark A. Wieczorek,[1] Gareth S. Collins,[2] Matthieu Laneuville,[1] Gregory A. Neumann,[3] H. Jay Melosh,[4] Sean C. Solomon,[5,6] Roger J. Phillips,[7] David E. Smith,[8] Maria T. Zuber[8]

Maps of crustal thickness derived from NASA's Gravity Recovery and Interior Laboratory (GRAIL) mission revealed more large impact basins on the nearside hemisphere of the Moon than on its farside. The enrichment in heat-producing elements and prolonged volcanic activity on the lunar nearside hemisphere indicate that the temperature of the nearside crust and upper mantle was hotter than that of the farside at the time of basin formation. Using the iSALE-2D hydrocode to model impact basin formation, we found that impacts on the hotter nearside would have formed basins with up to twice the diameter of similar impacts on the cooler farside hemisphere. The size distribution of lunar impact basins is thus not representative of the earliest inner solar system impact bombardment.

Progress in understanding impact basins on the Moon has been hampered by the simple fact that there is a lack of consensus on the size of the largest basins (*1*–*3*). From an impact physics perspective, the most relevant metric for the size of a basin is the diameter of its transient cavity, but as its name implies, this structure is short-lived and its diameter is not easily estimated from surface measurements (*4*). Most impact basins on the nearside hemisphere of the Moon have been filled by lava flows, hiding important morphological clues that could be used for determining the size of the transient cavity. Other impact basins have multiple rings, and it is unclear which of these, if any, most closely approximates the transient cavity. Because the impact process excavates large quantities of crustal material and uplifts mantle material beneath the basin center, an alternative metric for the size of a basin is the diameter of the region of crustal thinning (*5*–*7*). High-resolution gravity data obtained from NASA's Gravity Recovery and Interior Laboratory (GRAIL) mission (*8*) have provided global maps of crustal thickness on the Moon (*9*) that allow for an unambiguous determination of the region of crustal thinning for all impact basins with diameters greater than 200 km.

GRAIL gravity data show that lateral variations in the Moon's crustal thickness are dominated by impact basins ranging in diameter from ~200 to 2000 km (*9*). Approximately half of those basins formed in the Imbrian and Nectarian periods, from ~3.7 to perhaps 4.2 billion years ago (Ga) (*10*, *11*) (table S1). The sole exception is the South Pole–Aitken basin, which is the oldest and largest impact structure on the Moon, and which we do not consider further on the grounds that it likely formed during a much earlier epoch than the other basins for which variations in crustal thickness have been preserved. We quantify the size of lunar impact basins by the diameter *D* of the region of crustal thinning (*1*). There are 12 basins on each hemisphere with diameters greater than 200 km and crust thinned to a few kilometers, as resolved by GRAIL (Fig. 1). Although the total number of basins is equal on the two hemispheres, their size distribution is highly asymmetric (Fig. 2). Whereas there are eight basins on the nearside hemisphere with diameters greater than 320 km, only one of this size is found on the farside, and this basin (Orientale, 94°W, 20°S) straddles the western limb of the Moon. Simulations of the Moon's impact bombardment by near-Earth asteroids show that the difference in cratering rate between the nearside and farside hemispheres should be less than 1% (*12*) for a large range of impact conditions. With a uniform cratering rate, there is less than 2% probability that eight basins with diameters greater than 320 km would form on the nearside and only one such basin on the farside (fig. S1).

The Moon shows major geological differences between the nearside and farside hemispheres. The nearside is dominated by the compositionally unique Procellarum KREEP Terrane (PKT), which is highly enriched in heat-producing and other incompatible elements [potassium, rare-earth elements, and phosphorus (KREEP)] that likely formed during the late stages of magma-ocean crystallization (*13*, *14*) (Fig. 1). More than 99% by area of the Moon's exposed basaltic lavas erupted on the lunar nearside; this concentration has been attributed to higher than average nearside mantle temperatures, at least in part the result of the high concentration of heat-producing elements in the nearside crust and upper mantle (*15*). The evidence for viscous relaxation of topographic relief of nearside basins (*16*, *17*) and the presence of mare basalts extending beyond the confines of the surface area of thorium enrichment (which defines the PKT) suggest that higher than average subsurface temperatures surrounded

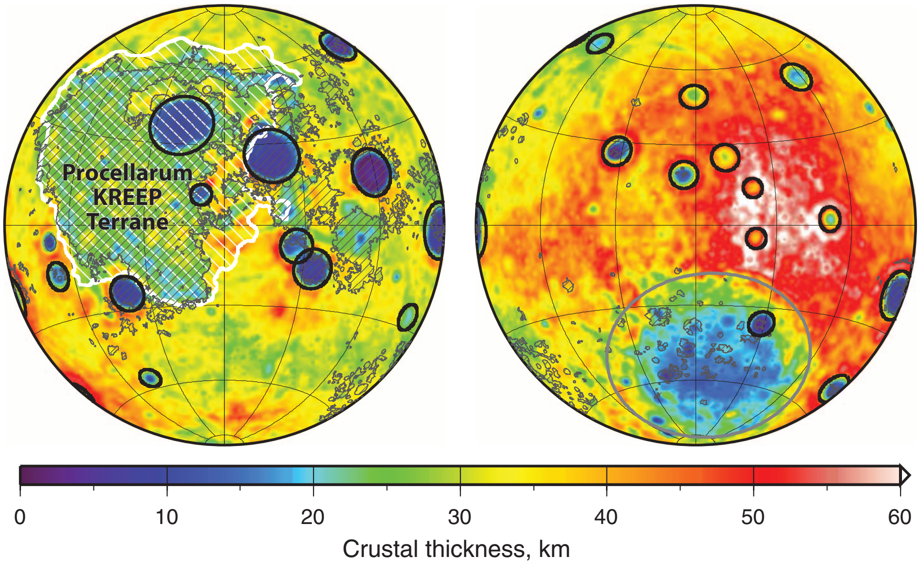

Fig. 1. Global map of crustal thickness on the Moon derived from GRAIL gravity data. Shown is the Procellarum KREEP Terrane (PKT; white cross-hatching), defined by the 4-ppm contour of thorium (*32*), and the distribution of mare basalt (black cross ruling). Excluding the South Pole–Aitken basin (gray circle), there are 12 impact basins with diameters of crustal thinning greater than 200 km (black circles) on each hemisphere. This image is presented in two hemispherical Lambert azimuthal equal-area projections centered over the nearside (left) and farside (right) hemispheres.

---

[1] Institut de Physique du Globe de Paris, Sorbonne Paris Cité, Université Paris Diderot, Case 7011, Lamarck A, 5, 35 rue Hélène Brion, 75205 Paris cedex 13, France. [2] Department of Earth Sciences and Engineering, Imperial College London, South Kensington Campus, London SW7 2AZ, UK. [3] Solar System Exploration Division, NASA Goddard Space Flight Center, Greenbelt, MD 20771, USA. [4] Department of Earth, Atmospheric, and Planetary Sciences, Purdue University, West Lafayette, IN 47907, USA. [5] Department of Terrestrial Magnetism, Carnegie Institution of Washington, Washington, DC 20015, USA. [6] Lamont-Doherty Earth Observatory, Columbia University, Palisades, NY 10964, USA. [7] Planetary Science Directorate, Southwest Research Institute, Boulder, CO 80302, USA. [8] Department of Earth, Atmospheric and Planetary Sciences, Massachusetts Institute of Technology, Cambridge, MA 02139, USA.

*Corresponding author. E-mail: miljkovic@ipgp.fr

the PKT for a considerable interval of lunar history. Several models have been proposed to account for the hemispheric differences in volcanic activity and heat-producing elements, all of which predict hemispheric differences in crustal and upper mantle temperatures (*15*, *18*–*20*). We propose that hemispheric differences in subsurface temperature and, to a lesser extent, crustal thickness (*9*) are the cause of the asymmetric distribution of large impact basins. We tested this hypothesis using numerical simulations of impact basin formation.

To investigate the consequences of impact basin formation on the two lunar hemispheres, we used the iSALE-2D shock-physics hydrocode (*21*–*23*). Vertical impacts onto the lunar surface were modeled with impact speeds of 10 and 17 km s^{-1}. From available material models and following previous work (*24*, *25*), we used basalt and dunite to represent the lunar crust and mantle, respectively, and dunite to represent the impactor (table S2). The pre-impact crustal thicknesses for the nearside and farside were set to 30 and 60 km, respectively. Representative subsurface temperature profiles beneath the nearside PKT and the farside hemisphere during the basin-forming epoch (4 Ga) were obtained from a three-dimensional thermochemical convection code (*26*) that included the asymmetric heat source distribution associated with the PKT (*20*) and provided results similar to those of previous asymmetric models (*15*) (fig. S2). For a given impact velocity and impactor diameter, six impact simulations were performed, each with different temperature profiles for each hemisphere (tables S3 and S4).

Our simulations show that lunar impact basins form via the growth of a deep, bowl-shaped transient cavity that is gravitationally unstable and that collapses by a combination of uplift of the crater floor and inward collapse of the crater rim (*7*, *25*). The crustal structure is modified in several ways during this process (fig. S4). During the formation of the transient crater, crustal material is ejected from inside the transient crater rim and deposited outside the transient crater; this process thins the crust inside the crater rim and thickens it outside (fig. S4). Because the size of the transient crater is limited by the impact energy available to displace the excavated mass in the ambient gravity field, the diameter of crustal thinning at this intermediate stage depends primarily on the impactor mass and speed and only weakly on the ambient temperature or crustal thickness. However, the subsequent collapse of the transient crater, and the consequent modifications in crustal structure, depend sensitively on the shear strength of the crust and upper mantle, which is a strong function of temperature. On the cooler and stronger farside, as the mantle beneath the crater floor is uplifted, crust beneath the transient crater rim collapses inward, forming a collar of crust around the mantle uplift and resulting in a diameter of thinned crust that is smaller than the transient crater diameter. In contrast, the collapse of the transient crater on the warmer and weaker nearside is more extensive: The mantle below the crater floor is uplifted farther and over a much broader region, which prevents the thickened crust surrounding the transient crater from collapsing back into the crater. As a result, the diameter of crustal thinning is substantially larger on the hot nearside than on the cold farside (Fig. 3).

The diameter of crustal thinning for a lunar basin formed in the nearside thin crust is plotted in Fig. 4 as a function of the diameter that would occur for the same impact in the farside thick crust. The crustal thinning diameter does not differ markedly between the two hemispheres when the same temperature profile is used. Nevertheless, as demonstrated by crustal thickness profiles in Fig. 3, the ambient crustal thickness does have an influence on the character of the final crustal thickness profile. In contrast, for the same impact conditions, the crustal thinning diameter is greatly affected by temperature profile. Despite forming a nearly identical transient cavity, nearside basins formed in a hot target can have diameters of thinned crust with up to twice the diameter of

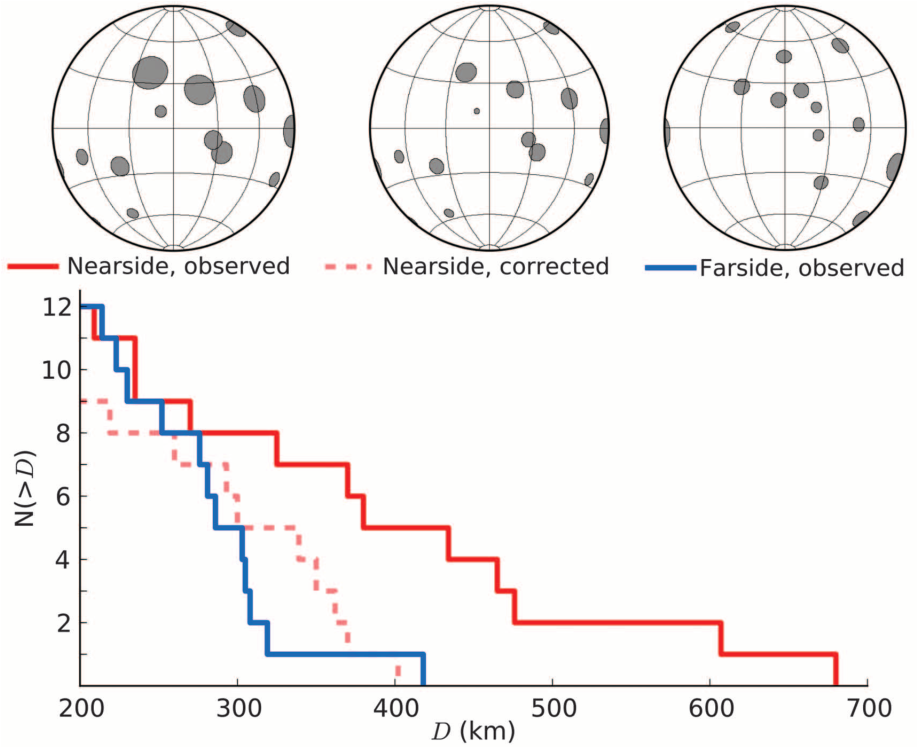

Fig. 2. Cumulative size distribution of observed lunar impact basins with diameters of crustal thinning *D* greater than 200 km for both hemispheres. The nearside is shown in solid red, the farside in solid blue. The size distribution of nearside basins after correction for lateral variations in target properties is shown in dashed red. Hemispherical maps depict the sizes and locations of basins used in the size-frequency distributions.

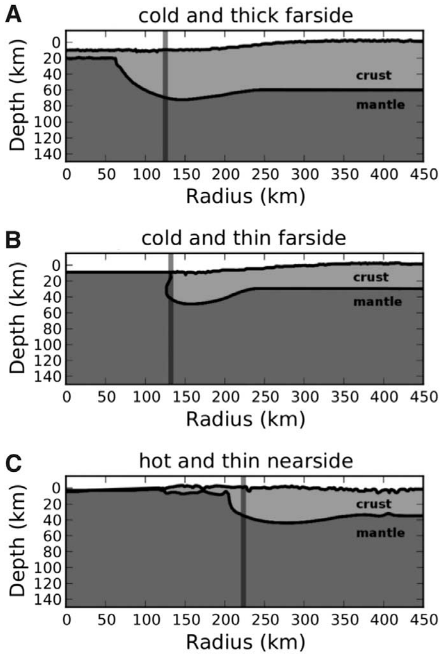

Fig. 3. Vertical cross sections of final surface topography and depth of the crust-mantle interface for three simulations of lunar impact basin formation. (**A** to **C**) Different temperature profiles for the farside [(A) and (B)] and nearside (C) correspond to the lunar thermal state at 4 Ga (M1/PKT1, fig. S2). Pre-impact crustal thicknesses were 60 km (A) and 30 km [(B) and (C)]. The basins were formed by the vertical impact of a 45-km-diameter projectile at an impact speed of 17 km s^{-1} onto the Moon. The diameter of crustal thinning *D* shown by the vertical lines is the radial distance from basin center at which the crustal thickness reaches the pre-impact value.

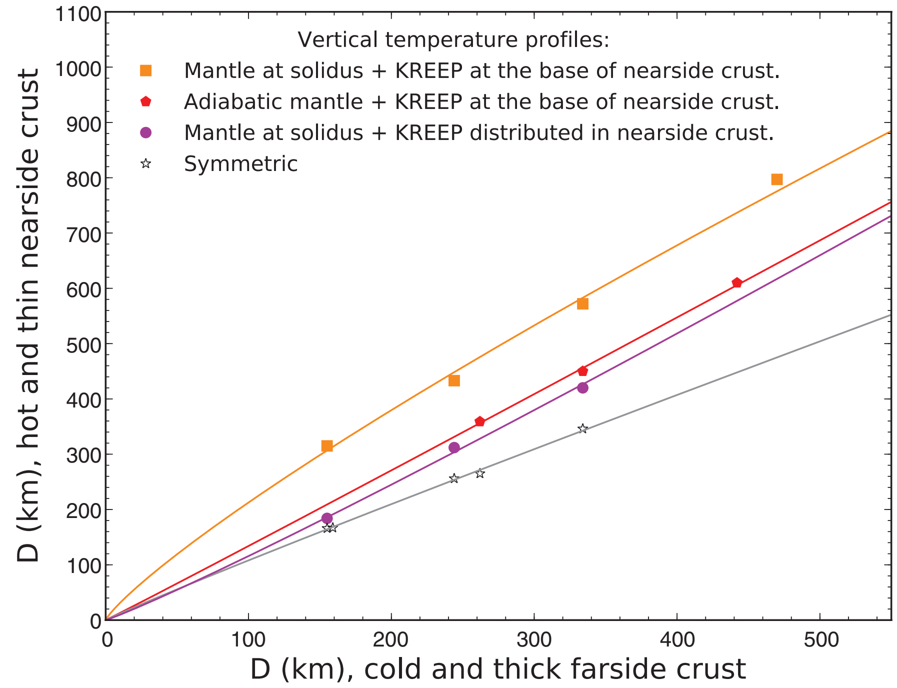

Fig. 4. Dependence of impact basin size on target properties. The ordinate is the diameter of crustal thinning *D* for a basin formed in a hot (KREEP-enriched) and 30-km-thick crust, and the abscissa is *D* for a basin formed in a cold and 60-km-thick crust, for the same size impactor. Points of the same color correspond to simulations with different projectile diameters. Variations for a given color reflect the different temperature profiles assumed for the nearside and farside; orange denotes the hottest temperature profile for the nearside (M1/PKT1, fig. S2) and violet denotes the coolest (M1/PKT2, fig. S2). The results in gray stars show *D* when the same temperature profile is used for both thin and thick crust.

the respective farside basins formed under similar conditions but in cold crust. These relationships between the diameter of crustal thinning on the nearside and farside hemispheres are largely independent of impact speed (from 10 to 17 km/s) and do not depend on differences in time of basin formation of up to a few hundred million years (fig. S3, table S4, and supplementary text).

The empirical relations from Fig. 4 can be used to compensate for the increase in basin size that results from lateral variations in target properties. Given that the absolute ages of most large lunar basins are poorly known, and that the subsurface temperature profile will vary both with time and distance from the PKT, such an exercise will be somewhat qualitative. We assumed that basins located within the PKT formed in the hottest and thinnest crust, and that basins surrounding the PKT formed in crust of intermediate temperature and thickness, and we then corrected the sizes of these basins to those that would be expected for impacts into the temperature regime of the colder farside highlands (supplementary text). Once lateral variations in target properties are included, Fig. 2 shows that the size distributions of impact basins on the nearside and farside hemispheres are comparable.

The concept of the late heavy bombardment (a spike in the impact cratering rate at ~4 Ga) (*27*–*29*) is based largely on the nearside impact basins that are either within or adjacent to the PKT. The temperature profile beneath this region is not representative of the Moon as a whole, and the special nature of the lunar nearside implies that the magnitude of basin-forming impact bombardment has been overestimated, mainly with respect to the impactor mass flux. The size distribution of impact basins on the farside hemisphere of the Moon is a more accurate indicator of the impact history of the inner solar system than that on the nearside. Lateral variations in target properties could have affected the size distribution of impact basins on other planets, such as Mars, which possesses a marked dichotomy in crustal thickness between the northern lowlands and southern highlands. A different temperature profile, combined with lateral variations in crustal temperature (*30*), could be responsible for the lower density of large impact basins on Mercury (*31*) than on the Moon, and higher surface temperatures are likely to have played an important role in determining the final sizes of craters on Venus.

References and Notes

1. M. A. Wieczorek, R. J. Phillips, *Icarus* **139**, 246–259 (1999).
2. H. Hikida, M. A. Wieczorek, *Icarus* **192**, 150–166 (2007).
3. C. I. Fassett *et al.*, *J. Geophys. Res.* **117**, E00H06 (2012).
4. E. P. Turtle *et al.*, in *Large Meteorite Impacts III*, T. Kenkmann, F. Hörz, A. Deutsch, Eds. (Geological Society of America, Boulder, CO, 2005), pp. 1–24.
5. G. A. Neumann, M. T. Zuber, D. E. Smith, F. G. Lemoine, *J. Geophys. Res.* **101**, 16841–16863 (1996).
6. S. R. Bratt, S. C. Solomon, J. W. Head, C. H. Thurber, *J. Geophys. Res.* **90**, 3049–3064 (1985).
7. R. Potter, D. A. Kring, G. S. Collins, W. Kiefer, P. McGovern, *Geophys. Res. Lett.* **39**, L18203 (2012).
8. M. T. Zuber *et al.*, *Science* **339**, 668–671 (2013).
9. M. A. Wieczorek *et al.*, *Science* **339**, 671–675 (2013).
10. M. D. Norman, R. A. Duncan, J. J. Huard, *Geochim. Cosmochim. Acta* **74**, 763–783 (2010).
11. V. A. Fernandes, J. Fritz, B. P. Weiss, I. Garrick-Bethell, D. L. Shuster, *Meteorit. Planet. Sci.* **48**, 241–269 (2013).
12. M. Le Feuvre, M. A. Wieczorek, *Icarus* **214**, 1–20 (2011).
13. B. L. Jolliff, J. J. Gillis, L. A. Haskin, R. L. Korotev, M. A. Wieczorek, *J. Geophys. Res.* **105**, 4197–4216 (2000).
14. R. L. Korotev, *J. Geophys. Res.* **105**, 4317–4346 (2000).
15. M. A. Wieczorek, R. J. Phillips, *J. Geophys. Res.* **105**, 20417–20430 (2000).
16. S. C. Solomon, R. P. Comer, J. W. Head, *J. Geophys. Res.* **87**, 3975–3992 (1982).
17. S. Kamata *et al.*, *J. Geophys. Res.* **118**, 398–415 (2013).
18. S. Zhong, E. M. Parmentier, M. T. Zuber, *Earth Planet. Sci. Lett.* **177**, 131–140 (2000).
19. P. C. Hess, E. M. Parmentier, *J. Geophys. Res.* **106**, 28023–28032 (2001).
20. M. Laneuville, M. A. Wieczorek, D. Breuer, N. Tosi, *J. Geophys. Res.* **118**, 1435–1452 (2013).
21. A. A. Amsden, H. M. Ruppel, C. W. Hirt, *SALE: A Simplified ALE Computer Program for Fluid Flow at All Speeds* (Report LA-8095, Los Alamos National Laboratory, 1980).
22. G. S. Collins, H. J. Melosh, B. A. Ivanov, *Meteorit. Planet. Sci.* **39**, 217–231 (2004).
23. K. Wünnemann, G. S. Collins, H. J. Melosh, *Icarus* **180**, 514–527 (2006).
24. E. Pierazzo, N. A. Artemieva, B. A. Ivanov, in *Large Meteorite Impacts III*, T. Kenkmann, F. Hörz, A. Deutsch, Eds. (Geological Society of America, Boulder, CO, 2005), pp. 443–457.
25. B. A. Ivanov, H. J. Melosh, E. Pierazzo, in *Large Meteorite Impacts and Planetary Evolution IV*, R. L. Gibson, W. U. Reimold, Eds. (Geological Society of America, Boulder, CO, 2010), pp. 29–49.
26. C. Hüttig, K. Stemmer, *Phys. Earth Planet. Inter.* **171**, 137–146 (2008).
27. F. Tera, D. A. Papanastassiou, G. J. Wasserburg, *Earth Planet. Sci. Lett.* **22**, 1–21 (1974).
28. D. A. Kring, B. A. Cohen, *J. Geophys. Res.* **107**, 5009 (2002).
29. K. Tsiganis, R. Gomes, A. Morbidelli, H. F. Levison, *Nature* **435**, 459–461 (2005).
30. J.-P. Williams, J. Ruiz, M. A. Rosenburg, O. Aharonson, R. J. Phillips, *J. Geophys. Res.* **116**, E01008 (2011).
31. C. I. Fassett *et al.*, *J. Geophys. Res.* **117**, E00L08 (2012).
32. D. J. Lawrence *et al.*, *J. Geophys. Res.* **108**, 5102 (2003).

Acknowledgments: Supported by UnivEarthS LabEx project of the University of Sorbonne Paris Cité grants ANR-10-LABX-0023 and ANR-11-IDEX-0005-02 (K.M.), UK Science & Technology Facilities Council grant ST/J001260/1 (G.S.C.), and the French Space Agency (CNES). The GRAIL mission is supported by the Discovery Program of NASA and is performed under contract to the Massachusetts Institute of Technology and the Jet Propulsion Laboratory, California Institute of Technology. We gratefully acknowledge the developers of iSALE-2D/3D (www.isale-code.de).

Supplementary Materials

www.sciencemag.org/content/342/6159/724/suppl/DC1
Supplementary Text
Figs. S1 to S4
Tables S1 to S5
References (*33*–*55*)

15 July 2013; accepted 30 September 2013
10.1126/science.1243224